Maccaferri, Nicolò; Berger, Andreas; Bonetti, Stefano; Bonanni, Valentina; Kataja, Mikko; Qin, Qi Hang; van Dijken, Sebastiaan; Pirzadeh, Zhaleh; Dmitriev, Alexandre; Nogués, Josep; Åkerman, Johan; Vavassori, Paolo

# Tuning the magneto-optical response of nanosize ferromagnetic Ni disks using the phase of localized plasmons

*Published in:*
Physical Review Letters

*DOI:*
10.1103/PhysRevLett.111.167401

Published: 01/01/2013

*Document Version*
Publisher's PDF, also known as Version of record

*Please cite the original version:*
Maccaferri, N., Berger, A., Bonetti, S., Bonanni, V., Kataja, M., Qin, Q. H., van Dijken, S., Pirzadeh, Z., Dmitriev, A., Nogués, J., Åkerman, J., & Vavassori, P. (2013). Tuning the magneto-optical response of nanosize ferromagnetic Ni disks using the phase of localized plasmons. *Physical Review Letters*, *111*(16), [167401]. https://doi.org/10.1103/PhysRevLett.111.167401

# Tuning the Magneto-Optical Response of Nanosize Ferromagnetic Ni Disks Using the Phase of Localized Plasmons

Nicolò Maccaferri,[1] Andreas Berger,[1] Stefano Bonetti,[2] Valentina Bonanni,[3] Mikko Kataja,[4] Qi Hang Qin,[4] Sebastiaan van Dijken,[4] Zhaleh Pirzadeh,[5] Alexandre Dmitriev,[5] Josep Nogués,[6,7] Johan Åkerman,[8] and Paolo Vavassori[1,9,*]

[1]*CIC nanoGUNE Consolider, 20018 Donostia-San Sebastian, Spain*
[2]*Department of Physics, Stanford University and Stanford Institute for Materials and Energy Science (SIMES), SLAC National Accelerator Laboratory, Stanford, California 94305-2004, USA*
[3]*CNR-ISTM and INSTM, 20133 Milano, Italy*
[4]*NanoSpin, Department of Applied Physics, Aalto University School of Science, FI-00076 Aalto, Finland*
[5]*Department of Applied Physics, Chalmers University of Technology, 41296 Gothenburg, Sweden*
[6]*ICN2–Institut Catala de Nanociencia i Nanotecnologia, Campus UAB, 08193 Bellaterra (Barcelona), Spain*
[7]*ICREA–Institució Catalana de Recerca i Estudis Avançats, 08010 Barcelona, Spain*
[8]*Materials Physics, School of Information and Communication Technology, KTH Royal Institute of Technology, Electrum 229,164 40 Kista, Sweden and Physics Department, University of Gothenburg, 412 96 Gothenburg, Sweden*
[9]*IKERBASQUE, Basque Foundation for Science, 48011 Bilbao, Spain*

(Received 10 July 2013; published 14 October 2013)

We explore the influence of the phase of localized plasmon resonances on the magneto-optical activity of nanoferromagnets. We demonstrate that these systems can be described as two orthogonal damped oscillators coupled by the spin-orbit interaction. We prove that *only* the spin-orbit induced transverse plasmon plays an active role on the magneto-optical properties by controlling the relative amplitude and phase lag between the two oscillators. Our theoretical predictions are fully confirmed by magneto-optical Kerr effect and optical extinction measurements in nanostructures of different size and shape.

DOI: 10.1103/PhysRevLett.111.167401 PACS numbers: 78.20.Ls, 73.20.Mf, 75.75.−c, 78.67.Bf

The investigation of the interaction between magneto-optical (MO) activity and plasmons has been a topic of enormous interest over the last three decades [1–17]. Current advances in nanostructuring make it nowadays possible to design new classes of nanosystems combining magnetic and plasmonic functionalities [18,19]. As a result, investigations of localized plasma resonances (LPRs) in such nanostructured systems are broadening our understanding of optics at the nanoscale. It has recently been shown that purely ferromagnetic nanostructures support LPRs [20]. They are, thus, an ideal playground for studying effects arising from the excitation of LPRs and the simultaneous presence of MO activity. Initial studies on these structures were mainly focused on the enhancement of MO effects (complex Kerr or Faraday rotation angle) [21–31]. Recent experimental investigations of the MO Kerr effect in systems made of Ni nanostructures have shown a plasmon-induced manipulation of the light phase that modifies the polarization of the reflected light. This effect can be exploited to achieve a controlled sign reversal of MO Kerr rotation or ellipticity through the engineering of the nanostructures dimension and shape [32,33]. MO activity originates from spin-orbit (SO) coupling and is an intrinsic property of a material that cannot be freely and easily controlled. These recent investigations shifted the paradigm of research on magnetoplasmonic functional materials by showing that the excitation of LPRs provides a pathway for tuning the MO response of a system beyond what is offered by the control of intrinsic material properties.

In this Letter, we show that the complex interplay between MO activity and LPRs in ferromagnetic nanostructures can be described in terms of a simple model based on two orthogonal damped harmonic oscillators coupled by the SO interaction. We confirm experimentally the validity of our model and demonstrate unambiguously that it is the LPR excited *transverse* to the electric field of the incident light by the *spin-orbit coupling* that governs the MO response observed in ferromagnetic nanostructures. Also, we show that the LPR directly excited by the electric field of the incident light is irrelevant for the MO response.

At first, we investigate three samples made of Ni circular nanodisks of average diameters $D = 70(\pm 5)$, $100(\pm 5)$, and $160(\pm 4)$ nm, and with filling factor around 10%. The nanodisks have the same thickness $t = 30$ nm and were fabricated on glass substrates into large-scale disordered arrays using hole mask colloidal lithography [34]. Scanning electron microscopy (SEM) images of such arrays are shown in the insets of Fig. 1(a). Figure 1(a) shows the far-field extinction spectra $(I_0 - I_t)/I_0$ of the three samples, where $I_0$ and $I_t$ are the intensities of the incident and transmitted light. The extinction spectra display the characteristic peak due to the excitation of a LPR at optical wavelengths as well as the expected redshift of the peak position with increasing nanodisk diameter.

 

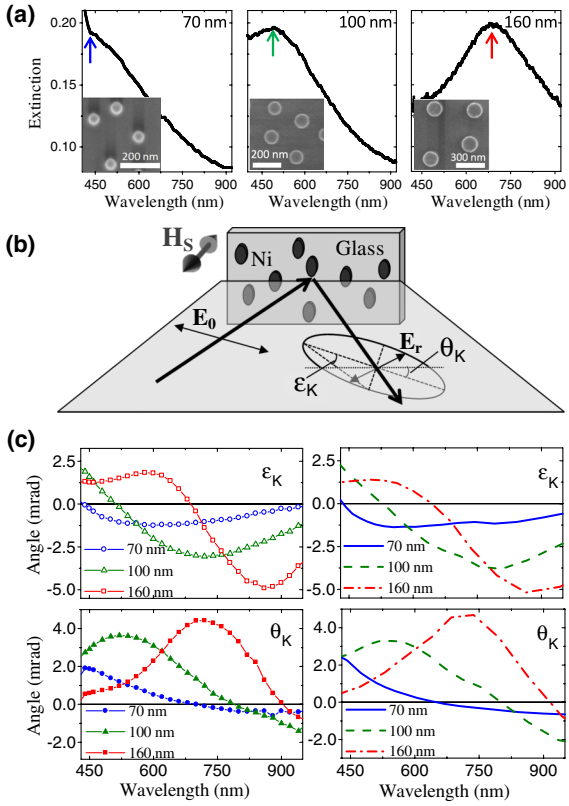


FIG. 1 (color online). (a) Extinction spectra of the three samples. The arrows mark the excitation of a plasmonic resonance. The insets show scanning electron microscopy images of a portion of each sample. (b) Schematic of the P-MOKE experiment. (c) Experimental (left panel) and calculated (right panel) P-MOKE spectra.

We performed MO Kerr effect (MOKE) reflectivity measurements in a Kerr spectrometer working in polar geometry (P-MOKE, incident angle 2.5°) in the wavelength range 420–950 nm. This is sketched in Fig. 1(b), together with the Kerr rotation ($\theta_K$) and ellipticity ($\varepsilon_K$) angles measured when the polarity of the saturating magnetic field $H_s = 8$ kOe was switched along the normal of the sample plane. $\theta_K$ and $\varepsilon_K$ were measured at each wavelength with the reflected beam passing through a photoelastic phase modulator and a polarizer before detection. Two lock-in amplifiers were used to filter the signal at the modulation frequency and at twice the modulation frequency in order to retrieve $\varepsilon_K$ and $\theta_K$ simultaneously [35].

The left column of Fig. 1(c) shows the P-MOKE spectra measured from the three specimens. A sign reversal of $\varepsilon_K$ can be observed in all three samples at the increasing wavelength of ~440, ~510, and of ~690 nm for $D$ of 70, 100, and 160 nm, respectively. At a wavelength close to that corresponding to each $\varepsilon_K$ sign reversal, a maximum of $\theta_K$ is observed, in agreement with the Kramers-Kronig relations. The comparison between the P-MOKE and extinction spectra clearly indicates that the features in the Kerr spectra are correlated to the excitation of LPRs in the Ni nanodisks.

The MO activity is due to SO interaction that couples transverse magnetic (TM or $p$) and transverse electric (TE or $s$) modes in the material. By impinging on the sample surface with a TM radiation, as sketched in Fig. 1(b), the reflected light acquires a small TE component, whose amplitude and phase lag $\phi$ with respect to the main TM component, determine the angles $\theta_K$ and $\varepsilon_K$ that identify the elliptical polarization of the reflected field. A vanishing $\varepsilon_K$ is observed when $\phi$ between TE and TM components of the reflected field is an integer multiple of $\pi$. Conversely, $\theta_K$ vanishes when $\phi$ is an odd integer multiple of $\pi/2$.

In order to precisely identify the physical mechanism through which the excitation of a LPR acts upon $\phi$, we model the collective oscillation of conduction electrons of a Ni nanodisk as two orthogonal damped harmonic oscillators coupled by the SO interaction, as sketched in Fig. 2. The nanodisk is approximated by an oblate ellipsoid with principal axes $D$ and $t$, and we assume that the electric field of the incident light is uniform over the disk volume.

We describe the optical properties of Ni with an antisymmetric permittivity tensor with $\varepsilon_{xx} \approx \varepsilon_{yy} \approx \varepsilon_{zz} \approx \varepsilon$ and $\varepsilon_{xy} = -\varepsilon_{yx} = -i\varepsilon Q$, where $Q$ is the Voigt parameter. All the remaining components of the tensor are equal to zero in the case considered here (disk magnetized along the $z$ direction). The off diagonal terms $\varepsilon_{xy}$ and $\varepsilon_{yx}$ account for the effects of the SO interaction on the dielectric properties of the constituent material. In our oscillators model, these terms, hence the SO coupling, couple the two transverse oscillation modes: if one oscillator is excited, part of the oscillation is transferred to the other orthogonal oscillator. The amplitude and phase of the oscillation along $x$ that is transferred to the orthogonal oscillator are governed by the interplay between the coupling strength, the stiffness of the springs, and the damping constant along $y$. Referring to Fig. 2, the complex electric field amplitude $E^0$ of the incident light, assumed to be a plane monochromatic wave, is driving the collective oscillation of the conduction electrons along $x$. Consequently, a complex oscillating electric dipole $p_x = \chi_{xx} E_x^i = (\varepsilon - \varepsilon_m)E_x^i$ is induced. Here, $\varepsilon_m$ is the dielectric constant of the medium

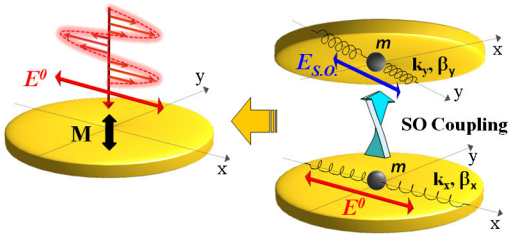


FIG. 2 (color online). A ferromagnetic disk modeled with two orthogonal damped harmonic oscillators coupled by the spin-orbit (SO) interaction; $m$ represents the mass of the conduction electrons; the spring constants $k_x$ and $k_y$ originate from the electromagnetic restoring forces due to the displacements of the conduction electrons; $\beta_x$ and $\beta_y$ are the damping constants.

surrounding the disk, $\chi_{xx}$ is the diagonal component of the electric susceptibility tensor $\bar{\boldsymbol{\chi}} = (\bar{\boldsymbol{\varepsilon}} - \bar{\mathbf{I}}\varepsilon_m)$ of the medium, $\bar{\mathbf{I}}$ the identity tensor, $E_x^i = E^0 - E_x^d$ is the internal electric field effectively acting on the conduction electrons. $E_x^d$ is the depolarizing field (restoring force) generated by $p_x$ owing to the spatial confinement and it is opposite to $E^0$. It is customary to express $p_x$ in terms of $E^0$ as $p_x = \alpha_{xx}E^0$, where $\alpha_{xx}$ is the disk polarizability along $x$. The general expression of $\alpha_{ii}$ can be easily derived to be $\alpha_{ii} = [\varepsilon_m(\varepsilon - \varepsilon_m)]/[\varepsilon_m + N_{ii}(\varepsilon - \varepsilon_m)]$ [33,36]. Here, $N_{ii}$ is the depolarizing factor along the $i$th direction, which accounts for the finite size and shape of the disk. The SO coupling transfers the oscillation to the second oscillator along $y$.

Considering the pure material effect, viz., neglecting for the moment the spatial confinement along $y$, the SO coupling induces an oscillating dipole $p_y^{\mathrm{SO}} = \chi_{yx}E_x^i = \varepsilon_{yx}E_x^i$. It is convenient to describe this coupling through a second electric field $E_{\mathrm{SO}} = p_y^{\mathrm{SO}}/\chi_{yy} = p_y^{\mathrm{SO}}/(\varepsilon - \varepsilon_m)$ acting on the conduction electrons along $y$: $E_{\mathrm{SO}} = \varepsilon_{yx}E_x^i/(\varepsilon - \varepsilon_m)$. Introducing the restoring force along $y$ due to the spatial confinement, the electric dipole generated by the damped harmonic oscillation driven by $E_{\mathrm{SO}}$ is $p_y = \alpha_{yy}E_{\mathrm{SO}} = E_x^i(\alpha_{yy}\varepsilon_{yx})/(\varepsilon - \varepsilon_m)$, where $\alpha_{yy}$ is the nanodisk polarizability along $y$.

The polarization of the far field radiated in the $z$ direction by these two mutually orthogonal oscillating electric dipoles is given by the ratio [37]

$$\frac{p_y}{p_x} = \frac{\varepsilon_{yx}\alpha_{yy}}{(\varepsilon - \varepsilon_m)^2}. \quad (1)$$

The fundamental consequence of Eq. (1), owing to the presence of *only* $\alpha_{yy}$ at the numerator, is that the plasmon-induced enhancement and phase tuning of the MO response occur when a LPR is excited by the SO coupling along the direction of the *transverse* harmonic oscillator. Noteworthy, the direct excitation of a *longitudinal* LPR by the incident light is *irrelevant* for the P-MOKE effect.

Equation (1) can be used to obtain the polar Kerr rotation and ellipticity for an isolated nanostructure of a general shape as $\theta_K = \mathrm{Re}[p_y/p_x]$ and $\varepsilon_K = \mathrm{Im}[p_y/p_x]$. For an ellipsoidal particle of given material ($\bar{\varepsilon}$) and size, Eq. (1) requires calculation of the $\alpha_{ii}$, viz., of the depolarizing coefficients $N_{ii}$. The latter are the elements of a diagonal tensor, called depolarizing tensor, and have to be computed numerically. Details of these calculations for a general ellipsoidal particle can be found in literature [33,36]. For a direct comparison of our model predictions with the experimental P-MOKE spectra, we use the Maxwell-Garnett effective medium approximation (EMA) approach [38–40]. This approach models the nanodisks in the embedding medium, a mix of air and glass in our case, as a homogeneous film described by an effective permittivity tensor that contains the polarizabilities and the disks concentration [33]. We set $\varepsilon_m = 1.15$ and used the tabulated values of $\varepsilon$ and $Q$ for Ni [41,42]. Finally, we introduce the transfer matrix method (TMM) [43–45] to account for the glass substrate and evaluate the *far field* P-MOKE response. The P-MOKE spectra thus calculated are shown in the right panel of Fig. 1(c). An outstanding agreement is obtained between the calculated and measured spectra, using as input parameters only the sizes and densities of the disks taken from SEM images, and literature values for optical and MO constants of glass and Ni. This proves that our simple model captures the essential physics of the interplay between MO activity and light-matter coupling in spatially confined geometries.

We now focus on Eq. (1) to gain further insights of the detailed physical mechanism underlying the observed MO spectral features. An important quantity that can be retrieved from Eq. (1) is the phase lag between the TM and TE components of field radiated in the $z$ direction. This phase lag is responsible for the peculiarities in the $\theta_K$ and $\varepsilon_K$ spectra, and it can be expressed as

$$\phi\left[\frac{p_y}{p_x}\right] = \phi\left[\frac{\varepsilon_{yx}}{(\varepsilon - \varepsilon_m)^2}\right] + \phi[\alpha_{yy}] = \phi_{\mathrm{SO}} + \phi_{\alpha_{yy}}. \quad (2)$$

Figure 3(a) shows how the two phase contributions, $\phi_{\mathrm{SO}}$ (due to the intrinsic properties of the material) and $\phi_{\alpha_{yy}}$ (related to the excitation of a LPR along $y$), combine. Figure 3(a) analyzes in detail the case of the Ni disk with $D = 160$ nm. The plot of $\mathrm{Im}[\alpha_{yy}]$ (dashed line) is

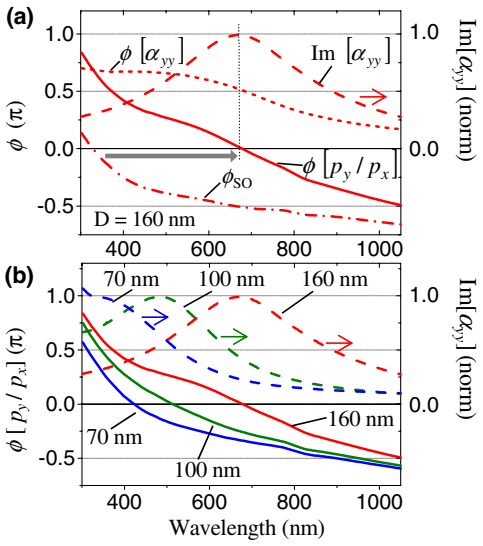


FIG. 3 (color online). Calculated spectral dependence of extinction ($\mathrm{Im}[\alpha_{yy}]$ normalized to 1, dashed line), total phase lag $\phi[p_y/p_x]$ between $p_y$ and $p_x$ electric dipoles (solid line), and individual phase contributions due to spin-orbit coupling ($\phi_{\mathrm{SO}}$, dot-dashed line) and plasmonic resonance ($\phi_{\alpha_{yy}}$, short-dashed line) for a Ni nanodisk with a diameter of 160 nm. The gray arrow shows the displacement of the point at which $\phi[p_y/p_x] = 0$ when the phase due to the plasmonic resonance is added to that due to the spin-orbit coupling. (b) Spectral dependence of extinction (dashed lines) and total phase lag $\phi[p_y/p_x]$ (solid lines) for three disk diameters.

proportional to the extinction efficiency for a single nanodisk and displays a peak at $\approx 680$ nm, in agreement with the corresponding experimental extinction spectrum shown in Fig. 1(a). The phase spectra of the LPR and SO contributions are plotted in the same figure (dotted and dash-dotted lines), together with their sum (solid line), which corresponds to the phase lag $\phi[p_y/p_x]$. The plot clearly shows that the additional phase, which is added by $\alpha_{yy}$ due to the LPR that is excited via $E_{SO}$, alters dramatically $\phi[p_y/p_x]$. Because of this contribution, the condition $\phi[p_y/p_x] = 0$, that results in a vanishing $\varepsilon_K$, redshifts from below 400 nm to 680 nm [gray arrow in Fig. 3(a)], in correspondence of the peak in the extinction spectrum. Figure 3(b) summarizes the spectral dependence of $\phi[p_y/p_x]$ for the three Ni disks (solid lines) together with their extinction efficiencies (dashed lines). Again, the wavelength at which $\phi[p_y/p_x] = 0$ is in excellent agreement with the wavelength of maximum extinction and sign reversal of $\varepsilon_K$ in the experimental spectra of Fig. 1(c) for all three nanodisks arrays.

So far, circular MO nanostructures have been considered where $\alpha_{xx} = \alpha_{yy}$ and LPRs were excited simultaneously in both $x$ and $y$ directions. This geometry is the most studied in literature and concealed, to date, the physical mechanism unveiled by Eqs. (1) and (2). In order to fully demonstrate that the direct excitation of a longitudinal LPR cannot give rise to the observed P-MOKE features, we investigated a sample in which the in-plane circular symmetry is broken, viz., the polarizabilities $\alpha_{xx}$ and $\alpha_{yy}$ are different. Such array is built from Ni nanoellipses with long and short axis of 180($\pm$10) and 100($\pm$5) nm, and a thickness of 30 nm. A SEM image of a portion of the array is shown in the inset of Fig. 4(a). Figure 4(a) displays the extinction spectra measured with the electric field $E^0$ of the incident light linearly polarized along the two in-plane symmetry axes of the system. Each spectrum shows a peak due to LPR with their maximum at 520 nm for $E^0$ along $y$ (short axis) and at 760 nm for $E^0$ along $x$ (long axis). In Fig. 4(b), we plot $\theta_K$ and $\varepsilon_K$ calculated using Eq. (1), viz., without including the glass substrate, and modeling the elliptical disk as an ellipsoid. The calculated spectra predict that, when $E^0$ is parallel to the *long* axis, $\varepsilon_K$ should vanish at the wavelength of the extinction peak observed when $E^0$ is applied along the *short* axis, and vice versa. In other words, the zero crossing of $\varepsilon_K$ is "blueshifted" when $E^0$ is parallel to the long axes, and redshifted when $E^0$ is parallel to the short axes. This result, counterintuitive at first sight, matches the physical picture developed so far that the LPR excited along the direction of the *transverse* harmonic oscillator, driven by the SO coupling, determines the peculiar spectral features in the P-MOKE spectra.

We now compare the prediction of Eqs. (1) and (2) with the experimental P-MOKE shown in Fig. 4(c). It is evident from the experimental data that the zero-crossing point for $\varepsilon_K$, as well as the $\theta_K$ maximum, when $E^0$ is applied along

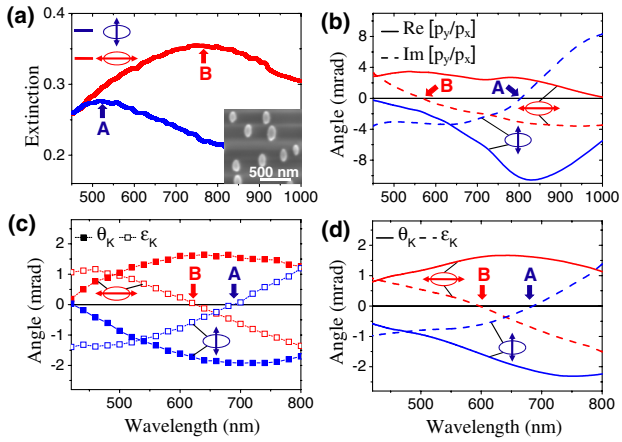


FIG. 4 (color online). (a) Extinction spectra of elliptical nanostructures for two directions of the incident electric field as sketched. The arrows $A$ and $B$ mark the peaks corresponding to the excitation of a plasmonic resonance. The inset shows a scanning electron microscopy image of a portion of the sample. (b) P-MOKE spectra, for two orientations of the electric field, calculated using Eq. (1). (c) Experimental P-MOKE spectra obtained for two electric field directions. (d) Calculated P-MOKE spectra for two electric field directions using Eq. (1) and the EMA-TMM approach.

the short axis ["$A$" in Fig. 4(c)] is "redshifted" compared to the case when $E^0$ is applied along the long axis ["$B$" in Fig. 4(c)], exactly as predicted by our model. Comparing Figs. 4(b) and 4(c), one could argue that for the case of ellipses, our model does not provide the same good quantitative agreement as for circular disks. However, the reason of the discrepancy is not related to the physics of the magneto-optics, rather it is due to the reduction of the P-MOKE contrast caused by the glass substrate. In order to prove that this is indeed the case, we again make use of the EMA-TMM approach to include the effect of the glass substrate. The results of these calculations are shown in Fig. 4(d), and the agreement with the experimental data is once again excellent. This proves that the apparent quantitative discrepancy between our model and the experimental data is merely a substrate effect, and directly confirms that our SO coupled two-oscillators model captures the essential underlying physics of the MO response of magnetoplasmonic nanostructures.

In conclusion, we investigated the spectral MO response of circular and elliptical Ni plasmonic nanostructures in polar configuration. By modeling the structures as two orthogonal damped harmonic oscillators coupled by SO interaction, we were able to unveil the fundamental physics that is responsible for the characteristic features in the MO spectra. Contrary to the intuitive argument that a MO enhancement is associated with the LPR that is directly excited by the electric field of the incident light, we demonstrated that the LPR excitation *transverse* to this electric field is what induces the observed MO spectral features. This result provides a new insight to the understanding of

magnetoplasmonic effects in nanostructures. Although devised for pure ferromagnetic nanostructures of simple shapes, the physical picture unveiled here applies to a broader class of nanostructures of complex shape and combining different materials, such as, e.g., multilayered and core-shell nanoparticles.

We thank for financial support the Basque Government (Program No. PI2012-47), the Catalan Government (Project No. 2009-SGR-1292), and the Spanish Ministry of Economy and Competitiveness (Projects No. MAT2012-36844 and No. MAT2010-20616-C02). S. B. and J. Å. acknowledge financial support from the Knut and Alice Wallenberg Foundation. Z. P., A. D., and J. Å. acknowledge the Swedish Research Council (VR) and the Swedish Foundation for Strategic Research, SSF (Z. P. and A. D.: Framework program Functional Electromagnetic Metamaterials, Project No. RMA08; J. Å.: Successful Research Leader Program). M. K., Q. H. Q, and S. v. D. acknowledge support from the National Doctoral Programme in Nanoscience and the Academy of Finland (Grant No. 263510).

*p.vavassori@nanogune.eu

[1] K. W. Chiu and J. J. Quinn, Phys. Rev. B **5**, 4707 (1972).
[2] P. E. Ferguson, O. M. Stafsudd, and R. F. Wallis, Physica (Amsterdam) **89B+C**, 91 (1977).
[3] P. M. Hui and D. Stroud, Appl. Phys. Lett. **50**, 950 (1987).
[4] H. Feil and C. Haas, Phys. Rev. Lett. **58**, 65 (1987).
[5] R. Nies and F. R. Kessler, Phys. Status Solidi (a) **111**, 639 (1989).
[6] V. I. Safarov, V. A. Kosobukin, C. Hermann, G. Lampel, J. Peretti, and C. Marlière, Phys. Rev. Lett. **73**, 3584 (1994).
[7] M. Abe and T. Suwa, Phys. Rev. B **70**, 235103 (2004).
[8] S. Tomita, T. Kato, S. Tsunashima, S. Iwata, M. Fujii, and S. Hayashi, Phys. Rev. Lett. **96**, 167402 (2006).
[9] V. I. Belotelov, L. L. Doskolovich, and A. K. Zvezdin, Phys. Rev. Lett. **98**, 077401 (2007).
[10] G. A. Wurtz, W. Hendren, R. Pollard, R. Atkinson, L. Le Guyader, A. Kirilyuk, Th. Rasing, I. I. Smolyaninov, and A. V. Zayats, New J. Phys. **10**, 105012 (2008).
[11] J. B. González-Díaz, A. García-Martín, J. M. García-Martín, A. Cebollada, G. Armelles, B. Sepúlveda, Y. Alaverdyan, and M. Käll, Small **4**, 202 (2008).
[12] V. V. Temnov, G. Armelles, U. Woggon, D. Guzatov, A. Cebollada, A. García-Martín, J. M. García-Martín, T. Thomay, A. Leitenstorfer, and R. Bratschitsch, Nat. Photonics **4**, 107 (2010).
[13] Z. Liu, L. Shi, Z. Shi, X. H. Liu, J. Zi, S. M. Zhou, S. J. Wei, J. Li, X. Zhang, and Y. J. Xia, Appl. Phys. Lett. **95**, 032502 (2009).
[14] V. I. Belotelov, I. A. Akimov, M. Pohl, V. A. Kotov, S. Kasture, A. S. Vengurlekar, A. V. Gopal, D. R. Yakovlev, A. K. Zvezdin, and M. Bayer, Nat. Nanotechnol. **6**, 370 (2011).
[15] J. C. Banthí, D. Meneses-Rodríguez, F. García, M. U. González, A. García-Martín, A. Cebollada, and G. Armelles, Adv. Mater. **24**, OP36 (2012).
[16] V. I. Belotelov *et al.*, Nat. Commun. **4**, 2128 (2013).
[17] J. Y. Chin, T. Steinle, T. Wehlus, D. Dregely, T. Weiss, V. I. Belotelov, B. Stritzker, and H. Giessen, Nat. Commun. **4**, 1599 (2013).
[18] V. V. Temnov, Nat. Photonics **6**, 728 (2012).
[19] G. Armelles, A. Cebollada, A. García-Martín, and M. U. González, Adv. Opt. Mater. **1**, 10 (2013).
[20] J. Chen *et al.*, Small **7**, 2341 (2011).
[21] W. Reim and D. Weller, Appl. Phys. Lett. **53**, 2453 (1988).
[22] T. Katayama, Y. Suzuki, H. Awano, Y. Nishihara, and N. Koshizuka, Phys. Rev. Lett. **60**, 1426 (1988).
[23] Y. Li, Q. Zhang, A. V. Nurmikko, and S. Sun, Nano Lett. **5**, 1689 (2005).
[24] J. B. González-Díaz, A. García-Martín, G. Armelles, D. Navas, M. Vázquez, K. Nielsch, R. B. Wehrspohn, and U. Gösele, Adv. Mater. **19**, 2643 (2007).
[25] P. K. Jain, Y. Xiao, R. Walsworth, and A. E. Cohen, Nano Lett. **9**, 1644 (2009).
[26] E. Th. Papaioannou, V. Kapaklis, P. Patoka, M. Giersig, P. Fumagalli, A. García-Martín, E. Ferreiro-Vila, and G. Ctistis, Phys. Rev. B **81**, 054424 (2010).
[27] G. X. Du, T. Mori, S. Saito, and M. Takahashi, Phys. Rev. B **82**, 161403 (2010).
[28] A. A. Grunin, A. G. Zhdanov, A. A. Ezhov, E. A. Ganshina, and A. A. Fedyanin, Appl. Phys. Lett. **97**, 261908 (2010).
[29] L. Wang, C. Clavero, Z. Huba, K. J. Carroll, E. E. Carpenter, D. Gu, and R. A. Lukaszew, Nano Lett. **11**, 1237 (2011).
[30] F. Wang, A. Chakrabarty, F. Minkowski, K. Sun, and Q. Wei, Appl. Phys. Lett. **101**, 023101 (2012).
[31] M. Rubio-Roy, O. Vlasin, O. Pascu, J. M. Caicedo, M. Schmidt, A. R. Goñi, N. G. Tognalli, A. Fainstein, A. Roig, and G. Herranz, Langmuir **28**, 9010 (2012).
[32] Valentina Bonanni, Stefano Bonetti, Tavakol Pakizeh, Zhaleh Pirzadeh, Jianing Chen, Josep Nogués, Paolo Vavassori, Rainer Hillenbrand, Johan Åkerman, and Alexandre Dmitriev, Nano Lett. **11**, 5333 (2011).
[33] N. Maccaferri *et al.*, Opt. Express **21**, 9875 (2013).
[34] H. Fredriksson, Y. Alaverdyan, A. Dmitriev, C. Langhammer, D. S. Sutherland, M. Zäch, and B. Kasemo, Adv. Mater. **19**, 4297 (2007).
[35] P. Vavassori, Appl. Phys. Lett. **77**, 1605 (2000).
[36] A. Moroz, J. Opt. Soc. Am. B **26**, 517 (2009).
[37] In Eq. (1), we neglect the back effect of $p_y$ onto $p_x$ that would lead to terms quadratic or higher order in $\varepsilon_{yx}$. This approximation is fully appropriate since $\varepsilon_{yx} \ll \varepsilon_{xx}$ in the spectral range considered here.
[38] J. C. M. Garnett, Phil. Trans. R. Soc. B **203**, 385 (1904).
[39] R. Landauer, J. Appl. Phys. **23**, 779 (1952).
[40] D. Stroud, Phys. Rev. B **12**, 3368 (1975).
[41] G. S. Krinchik and V. A. Artem'ev, Sov. Phys. JETP **26**, 1080 (1968).
[42] Š. Višňovský, V. Pařízek, M. Nývlt, P. Kielar, V. Prosser, and R. Krishnan, J. Magn. Magn. Mater. **127**, 135 (1993).
[43] M. Schubert, T. E. Tiwald, and J. A. Woollam, Appl. Opt. **38**, 177 (1999).
[44] J. Zak, E. R. Mook, C. Liu, and S. D. Bader, J. Magn. Magn. Mater. **89**, 107 (1990).
[45] Š. Višňovský, R. Lopusnik, M. Bauer, J. Bok, J. Fassbender, and B. Hillebrands, Opt. Express **9**, 121 (2001).